What [plasma used for growing] diamond can shine like flame?

Michael N.R. Ashfold,[1*] Edward J.D. Mahoney,[1] Sohail Mushtaq,[1] Benjamin S. Truscott [1] and Yuri A. Mankelevich [2]

[1] School of Chemistry, University of Bristol, Bristol, U.K. BS8 1TS.

[2] Skobel'tsyn Institute of Nuclear Physics, Lomonosov Moscow State University, Leninskie gory, Moscow, 119991 Russia

Abstract

Diamond synthesis by chemical vapour deposition (CVD) from carbon-containing gas mixtures has by now long been an industrial reality, but commercial interest and investment into the technology has grown dramatically in the last several years. This Feature Article surveys recent advances in our understanding of the gas-phase chemistry of microwave-activated methane/hydrogen plasmas used for diamond CVD, including that of added boron-, nitrogen-, and oxygen-containing dopant species. We conclude by considering some of the remaining challenges in this important area of contemporary materials science.

TOC entry and graphic

The gas-phase chemistry underpinning the chemical vapour deposition of diamond from microwave-activated methane/hydrogen plasmas is surveyed.

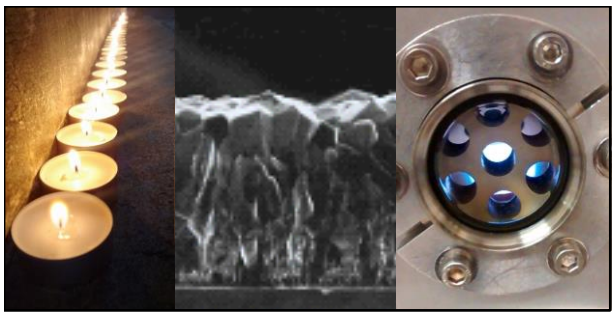

Introduction

Diamond, the sp^3-bonded allotrope of carbon, sits on a pedestal in the minds of students, scientists and the wider public. Diamond displays an impressive range of extreme material properties.[1,2] It defines the top end of Mohs' scale of mineral hardness and is chemically inert and radiation-hard, with a low coefficient of thermal expansion. It has very high dielectric strength, yet can be doped to become a semiconductor, metal, or even superconductor. It possesses the highest thermal conductivity of any solid close to room temperature, achieving a value of ~2000 W m^{-1} K^{-1}—some five times that of copper. It has an unprecedented range of optical transparency, extending from the ultraviolet (UV) into the far infrared (IR). Its high refractive index at visible wavelengths, $\eta \approx 2.4$ (*cf.* $\eta \approx 1.5$ for glass), makes it an interesting optical material and predisposes it to multiple internal reflections—which, combined with its moderate dispersion, are the source of the "fire" so prized in exactingly cut diamond gems. This, along with its durability and the scarcity of flawless natural specimens, has contributed to its long-held position among the most precious of gemstones.[3]

Faraday was not immune to the allure of diamond. As a 22-year-old assistant to Humphry Davy at the Royal Institution, he documented their "grand experiment" employing the sun's rays and the Grand Duke of Tuscany's burning-glass (a Keplerian telescope) to ignite diamond in an oxygen atmosphere, hence proving, after Davy's analysis of the combustion products, that it was comprised solely of carbon. The title of this Feature Article is adapted from Faraday's famous discourse on the *The Chemical History of a Candle*,[4] where he writes "It concerns us much to know about the condition which the matter of the candle finally assumes at the top of the wick, where you have such beauty and brightness as nothing but combustion or flame can produce. You have the glittering beauty of gold and silver, and the still higher lustre of jewels like the ruby and diamond; but none of these rival the brilliancy and beauty of flame. What diamond can shine like flame? It owes its lustre at night time to the very flame shining upon it. The flame shines in darkness, but the light which the diamond has is as nothing until the flame shines upon it, when it is brilliant again." Fittingly, we now know that the links between a combustion flame and diamond extend beyond a subjective comparison or a means of analysis, and that fire cannot only consume diamond, but also produce it. Nanodiamonds have been shown to form in the flame of a candle,[5] and the literature contains many reports of successful diamond growth from oxygen-hydrocarbon flames.[6-9]

The latter studies illustrate one of several different approaches to producing diamond from gas-phase precursors, all of which fall under the umbrella of chemical vapour deposition (CVD)

methods, the development of which for diamond growth began in the early 1980s.[10,11] Historically, the first reported laboratory synthesis of diamond employed *solid* precursors, reacted at high pressures and temperatures.[12] This forms the basis for the high-pressure high-temperature (HPHT) method, whereby diamond is crystallised from metal-solvated carbon at >5 GPa and >1500°C, under which conditions it is thermodynamically favored with respect to graphite. HPHT still accounts for most synthetic diamond production today. CVD methods, in contrast, rely on the production of *gas*-phase carbon-containing radical species close to a solid surface, from which diamond can be deposited as a kinetically stable product. Combustion flames, DC glow discharges [13-18] and DC plasma-jets [19-24] have all attracted passing interest, but most reported diamond CVD involves either hot filament or microwave plasma activation methods.[25-31]

In common among the CVD methods, the growth of diamond (rather than other, or mixed phases of carbon) typically requires that the substrate is held at a temperature (T_{sub}) in the range 1000–1400 K, and that the carbon-containing precursor (typically methane) is present at the level of a few percent in an excess of hydrogen. The H_2 plays several key roles as will be outlined in section 2. Pre-existing diamond can be used as a substrate, which is today the most common approach to producing single-crystal diamond by CVD. Because of the co-nucleation of multiple, randomly-oriented grains, diamond grown on other substrate materials will generally be polycrystalline, with a texture and morphology that depends on the chosen growth conditions. As Figure 1 shows, the average grain size in polycrystalline CVD diamond can be reduced from many microns to just a few nanometres, primarily by increasing the C/H ratio in the process gas mixture. Clearly, such nanocrystalline material contains many grain boundaries, and so exhibits the idealized characteristics of diamond to a lesser extent than does material made up of larger crystallites. Indeed, the sp^3/sp^2 ratio, readily assessed by Raman spectroscopy,[32,33] is commonly employed as a metric of polycrystalline diamond "quality".

The T_{sub} requirement severely limits the range of substrates upon which diamond can be grown, and in fact, the list of suitable materials is quite short. Substrates with low melting points, such as plastics, glass, and aluminium, are immediately ruled out. Many other metals (most notably iron) are also eliminated because of the extensive solubility of carbon within them, leading to preferential carburization. On the other hand, the formation of a thin, stoichiometric carbide layer at the interface, such as occurs with the refractory metals, is beneficial for the adhesion of CVD diamond to a substrate. Since diamond has a coefficient of thermal expansion much lower than that of any non-diamond substrate, once the sample has been returned to room

temperature after growth, the deposited diamond will be under compressive stress. Delamination may result. Such an outcome is desirable when the requirement is a freestanding diamond film or plate, but a challenge if the ambition is for the substrate to remain coated with diamond. These and related considerations (such as high thermal conductivity) have led to silicon, tungsten and molybdenum emerging as favoured substrate materials for diamond CVD.

As noted above, most contemporary diamond CVD employs either a hot filament (HF) or a microwave (MW) plasma to activate the gas mixture. In both cases, the activation mechanism is the thermal dissociation of H_2, but the plasma method is capable of achieving much higher temperatures within a larger volume and thus higher growth rate. If a filament is used, it must be held in close proximity to the substrate and maintained at a temperature >2000°C, whereupon surface-catalysed hydrogen decomposition yields H atoms.[34] The most common filament materials are W, Ta, or Re because of their high melting points. Laser and mass spectroscopic measurements of key species (including H atoms,[35-40] and CH_3 radicals [37,41,42]) in HF-activated CH_4/H_2 gas mixtures, coupled with thermodynamic and gas-kinetic modelling,[27,43] have yielded a fairly complete picture of the prevailing gas-phase chemistry. There are two key aspects to this picture. First, there is a large temperature gradient within the reactor volume, which drives the diffusion of H atoms away from the filament. The temperature of the gas (T_{gas}) very close to the HF is just a few hundred degrees below that of the HF surface, but declines to near room temperature at the reactor walls. Second, H_2 is a poor 'third body' for the H atom recombination reaction, and so many of the H atoms formed at the HF surface reach (and recombine at) the cool walls of the reactor. Conditions of high H atom number density and high T_{gas} drive the sequence of H-atom abstraction reactions shown in Figure 2 toward formation of CH_x ($x \leq 3$) and C_2H_y ($y \leq 6$) species. The rates of these abstraction reactions are sensitive functions of T_{gas}, however, and further from the HF (where $T_{gas} < 1500$ K), the overall scheme shown in Figure 2 reverses: the net conversion in the cooler regions is of C_2H_2 to CH_4, driven by (third-body stabilised) H-atom addition reactions.[27]

We will revisit these species inter-conversions when discussing MW activated CH_4/H_2 gas mixtures below. The key points to note at this stage are that (i) the CH_4 (or other hydrocarbon precursor) in the input gas mixture cycles through a series of CH_x and C_2H_y species and, almost certainly, heavier C_nH_z ($n > 2$) species in the cooler regions, though the latter are generally not explicitly included in the modelling; (ii) the concentrations of these various species will depend sensitively on the reactor design, location within the reactor, and the process conditions; and (iii) as a result, diamond growth requires that the substrate of choice is placed at a suitable

location within this processed gas mixture and maintained at an appropriate temperature (T_{sub}). We return later to consider what constitutes a suitable location.

2. Microwave Activated Gas Mixtures for Diamond CVD

From here on we focus on insights gained from *in situ* measurements and companion modelling of a custom designed MW reactor (2 kW, 2.45 GHz power supply), details of which can be found in previous publications.[44-46] Figure 3 shows an image of the operating reactor, along with a schematic cross-section. MW radiation is delivered through a rectangular waveguide, converted to the TM_{01} mode and coupled into the cylindrical chamber. The walls and base of the chamber are water cooled, and the chamber is divided by a centrally mounted quartz plate. The lower half of the chamber is vacuum sealed and contains the plasma. The inner diameter of this chamber is 12.0 cm, and the separation between the top of the substrate and the lower face of the quartz window is ~5.7 cm. The substrate – typically a 30 mm diameter, 3 mm thick Mo disc – sits on a thin spacer above the centre of the base plate. Varying the spacer thickness allows some control of substrate cooling and thus T_{sub}. The pre-mixed source gas is introduced through inlets located close below the quartz window and exhausted through the base plate. 'Base' operating conditions for most of the work reported here employed an input MW power P = 1.5 kW, a gas pressure p = 150 Torr and a total flow rate $F \approx 500$ standard cm^3 per minute (sccm). Necessarily, any detailed study of the plasma chemistry underpinning successful diamond CVD requires systematic variation of these and other parameters — most notably the process gas mixture.

The reactor is equipped with vertical slot-shaped viewports to allow laser probing of, and direct observation and imaging of spontaneous optical emission from, the full height of the plasma. Most recent advances in the diagnosis of diamond growing plasmas stem from the increased flexibility of laser absorption spectroscopy methods, which enable spatially resolved measurements of the column densities of target species as functions of the process conditions. Stable hydrocarbons like CH_4, C_2H_2 and C_2H_6, and CH_3 radicals, have all been monitored by direct line-of-sight IR absorption methods.[46-51] CH_3 radicals have also been monitored by line-of-sight absorption in the deep UV,[48,52] but our more recent absorption measurements of radical species in MW activated CH_4/H_2 gas mixtures (with or without added dopants) have all used cavity ring down spectroscopy (CRDS).[44,53-57]

Analysis of absorption data can yield *absolute* species number densities. What is generally measured, however, is the absorption of just a few of the populated quantum states of the target

species. Even in the case of a homogeneous sample, converting such line integrated absorption data into absolute column densities requires detailed knowledge of the relevant spectroscopy and transition moments at the sample temperature. The challenge is still greater in the case of the CVD plasma, since the probed column is inhomogeneous and spans a very wide range of T_{gas}. As shown below, the total number density in the plasma centre is typically an order of magnitude less than that near the reactor wall, and the gas chemistry and composition vary hugely along the probed column. To develop a thorough understanding of the process chemistry we thus require a combination of experiments *and* complementary theory. Experimental measurements are crucial for validating model calculations, but model outputs (*e.g.* the spatial variations of T_{gas} and the species mole fractions) are equally important for quantitative interpretation of the experimental data.

As seen in Figure 3, the plasma is luminous, and is thus amenable to analysis by optical emission spectroscopy (OES)—a technique that has long been employed for monitoring and optimizing plasma processes.[45,58-60] OES measures the emission from electronically excited species, which can be populated in a number of ways (chemiluminescent reactions, dissociative excitation, electron–ion recombination) but, most typically, by electron impact (EI) excitation of the ground–state species. Thus the emission intensities are intimately linked to the electron energy distribution function (EEDF), and can provide information about how the electron density (n_e) and temperature (T_e) vary with position and changes in process conditions.[45,60] High–resolution OES measurements can provide estimates of the temperature of the emitting species (through, for example, the Doppler broadening of lines in the Balmer series of atomic hydrogen or from the relative intensities of series of lines in the emission spectrum of H_2 or of the C_2 radical), which is often used as a proxy for the local T_{gas}. Actinometry, a variant of OES in which emission from a target species is measured in parallel with that from a small quantity of an inert tracer species (usually Ar), offers a route to determining the densities of, for example, ground state H atoms (a quantity that can be difficult to measure by laser based methods).[45,60]

Any thorough description of diamond-growing plasmas requires experimental measurements *and* theoretical modelling. Many inter-related phenomena must be accounted for to build a complete model of diamond growth in a MW CVD reactor. These include: the propagation of electromagnetic (EM) fields in the reaction chamber and their interaction with the plasma; the resulting non-equilibrium electron energy distribution; gas heating; heat and mass transfer; the many charged and neutral species involved in the vast array of plasma-chemical reactions for

realistic source gas mixtures (*i.e*. H/C, H/C/noble gas and H/C/dopant gas mixtures); excitation and radiation processes; species dependent diffusion and thermodiffusion; and a range of gas−surface processes. Accommodating all of these into a single simulation in a self-consistent manner is a massive challenge, and all models reported to date necessarily introduce simplifications. The (near) cylindrical symmetry of most MW reactors encourages use of a 2-D coordinate system (i.e. height above substrate *z*, and radius *r*) almost without loss of generality, but owing to the stiffness of the hydrocarbon chemistry, 2-D simulations including a realistic treatment of the EM field are, with one exception,[61] restricted to the case of pure H_2.[62-65] Since the electromagnetic coupling and losses do not vary much by the introduction of other gases in few-percent proportions, this restriction largely suffices for the study of reactor designs, leaving the detailed process chemistry—shared in common among all reactors of a general type—as a separate question.

It is this latter question that our Bristol-Moscow collaboration has sought to address, and we have generated 2-D kinetic and transport models for H/C and H/C/Ar plasmas, [66-69] as well as for H/B/Ar and H/C/B/Ar,[54,70] H/N and H/C/N,[57,71] and H/C/O [56,72] process mixtures, in all cases without explicit calculation of the EM fields. The other main elements of our model are incorporated in a self-consistent manner and describe: (i) power absorption and gas heating, and heat and mass transfer; (ii) plasma activation of the reactive gas mixture; the plasma-chemical kinetics, which involves calculation of non-Maxwellian EEDFs and the diffusion and thermodiffusion of neutral species; and ambipolar diffusion of the charged species; and (iii) gas−surface processes (diamond deposition, and the loss/production of atoms, radicals, ions and electrons). The rate coefficients for the various electron–atom and electron–molecule activation reactions depend on the local EEDF, which in a typical MW CVD plasma is a function of the reduced electric field *E*/*N*. We introduce two simplifying assumptions that remove the need to include the EM fields explicitly. First, we assume *E/N* (and so the average T_e) to be fairly uniform throughout the entire plasma region, and to fall steeply at the boundary of the plasma. Second, the size (radius r_{pl} and height h_{pl}) and shape of this plasma region, i.e. the geometry of the imposed electric field for our particular reactor, is treated as an external parameter in the model, and is chosen to faithfully reproduce all available experimental data. These simplifications allow the MW power absorption and the activation volume to be accommodated as parameters, and thus allow estimation of *E*/*N* and T_e in the plasma region for any given value of input power. The absorbed power density, *Q*, is then calculated directly as

a sum of power losses and gains associated with the various electron–particle reactions: electronic, vibrational and rotational excitation/de-excitation, dissociation, and ionization.

Quantities like n_e, T_{gas} and the charged species and radical densities show huge variations over the volume of any MW CVD reactor, which necessitates the use of a rather comprehensive plasma-chemical mechanism. By way of illustration, the basic plasma-chemical kinetic scheme used in our H/C/Ar plasma model [67] includes 30 neutral species, 8 charged species (electrons, and the ions $C_2H_2^+$, $C_2H_3^+$, H^+, H_2^+, H_3^+, Ar^+ and ArH^+) and >240 direct and reverse reactions. Clearly, the complexity increases yet further upon introducing B, N or O containing species, and one is continually challenged to make pragmatic decisions regarding what species/reactions require inclusion. The final stage in any simulation requires solution of the set of model equations in a self-consistent manner. In all of the simulation work presented hereafter, the non-stationary conservation equations for mass, momentum, energy and species concentrations have been solved numerically in (r, z) coordinates by a finite difference method, to provide spatial distributions of T_{gas}, species concentrations, power absorption and mass/energy transport. The 2-D model takes account of changes in plasma parameters and conditions (e.g. in T_{gas}, T_e, n_e, Q and the plasma chemistry) induced by varying reactor parameters like p, P, and the mole fractions of the various components in the process gas mixture.

We now illustrate key aspects of the plasma chemistry of a range of process gas mixtures, as determined by calibration of the associated models against experiment. We start with a brief summary of pure H_2 plasmas before progressing to consider the dilute CH_4/H_2 plasmas used for diamond CVD. In both cases, the MW field partially ionizes and dissociates the input gas mixture, which in the case of CH_4/H_2 plasmas undergoes further chemical processing to yield 'active' species that react at the proximal substrate surface to form a polycrystalline diamond film. Having established the chemistry prevailing in such CH_4/H_2 plasmas, we will then review how these (and the resulting diamond films) are affected by the addition of dopants like boron (introduced as diborane), nitrogen (as N_2) and oxygen (from CO_2), before briefly returning to highlight the recent identification of molecular anions in the base CH_4/H_2 plasma.

2.1 H_2 plasmas

The dominant pathway to H atom formation in a MW plasma depends on both p and T_{gas}. At low p, for example, most H atoms are formed by EI excitation of H_2 triplet states that radiate

to the repulsive $b^3\Sigma_u^+$ state.[73] With increasing p, however, the mean free path is reduced, collisional energy transfer from the electrons to H_2 causes more gas heating, and the H_2–H_2 collision frequency increases. For typical process pressures, p >100 Torr, T_{gas} becomes sufficient for thermal dissociation of H_2 to be the main route to producing H atoms.[63,67,71,74] The primary ionization mechanism also depends on the process conditions. Direct EI ionization of H_2 (1), the sets of reactions (2) and (3) involving the formation and ionization/excitation, respectively, of H atoms, and the ionization reaction (4) of electronically excited H atoms (H*) are all important for T_{gas} < 3000 K. At higher T_{gas}, and thus [H]/[H_2] > 5–10%, (1) becomes relatively less important. Electron loss is mainly by dissociative electron attachment to H_3^+, or by transport to the walls at low p.

$$H_2 + e \rightarrow H_2^+ + 2e \quad (1)$$

$$H_2 + M \leftrightarrow 2H + M \quad (\text{with } M = H, H_2) \quad (2a)$$

$$H_2 + e \rightarrow 2H + e \quad (2b)$$

$$H + e \rightarrow H^+ + 2e \quad (3a)$$

$$H + e \rightarrow H^* + e \quad (3b)$$

$$H^* + H_2 \rightarrow H_3^+ + e \quad (4)$$

MW power is absorbed preferentially near the substrate surface (due to the maximal electric field in that location) and this determines the local EEDF, which although not strictly Maxwellian, can be approximated by a Maxwellian temperature T_e along with a hyperthermal tail. The T_e distribution follows the absorbed power distribution closely, and the electron source terms are largely determined by T_e. The n_e distribution is of course sensitive to these source terms, but shows a less steeply varying spatial distribution, reflecting the importance of transport (ambipolar diffusion) in establishing the electron density balance. The T_{gas} distribution peaks further above the substrate surface than do T_e and n_e, reflecting the role of conduction and diffusion in transporting energy from the point of maximum power deposition, and declines to near room temperature at the water-cooled reactor walls. As shown in section 2.2, the large variation in T_{gas} within the reactor volume has major implications for any experimental diagnoses and for the modelling.

2.2 CH_4/H_2 plasmas

As noted above, adding a small amount of hydrocarbon to a H_2 plasma has relatively little effect on the EM field in the resonant cavity or the spatial distributions of the electron and ion

densities. At constant P, adding a few percent CH_4 will typically cause these distributions to shrink a little. This reflects the lower ionization potentials and thus greater ionization probabilities of the hydrocarbon components (principally C_2H_2; recall Figure 2) compared to H_2. Thus, n_e will increase in the presence of hydrocarbons, and H_3^+ will be supplanted by $C_2H_2^+$ and $C_2H_3^+$ as the most abundant ions in most MW-activated H/C CVD plasmas.[67,75]

The 2-D (r, z) false colour plots shown in Figure 4 illustrate several key features of these plasmas and highlight some of the aforementioned challenges to experimental diagnosis and to modelling. The displayed data are for a flowing gas mixture consisting of 4.4% CH_4, 7% Ar and 88.6% H_2, operating at our base conditions of p = 150 Torr and P = 1.5 kW, and quantities notated as […] and X(…) represent, respectively, number densities and mole fractions of the given species. The n_e distribution, Figure 4(a), determines the region within which MW power can be absorbed. The absolute n_e value in the plasma core is established by the local balance between the total ionisation rate, dominated by EI ionization of C_2H_2, and the rate of recombination of electrons with (mainly) $C_2H_y^+$ ions. This in turn dictates the T_{gas} distribution, Figure 4(b), which peaks at $T_{gas} \approx 2900$ K, and thus the H atom number density distribution, Figure 4(c), the corresponding mole fraction for which maximizes at ~8% under our chosen base conditions. $X(H_2)$ varies by just a few percent: $X(H_2) \approx 0.9$ in the plasma core and near the cooled reactor walls, maximizing at ≈0.95 in an annular shell around the plasma ball. However, as Figure 4(d) shows, the variation in T_{gas} ensures (via the ideal gas law) that [H_2] in the core region is almost an order of magnitude less than at the periphery of the reactor. Nonetheless, H_2 is still by far the majority species in the plasma core, with [H_2] some 6 orders of magnitude greater than n_e. Thus, these plasmas are weakly ionized even in the core, and can largely be understood as hot gas with a chemical composition that is determined by thermal chemistry.

The Ar tracer illustrates a further complication. Ar constitutes 7% of the input gas mixture in this simulation, but as shown in Figure 4(e), the calculated X(Ar) ranges from ≈2.7% in the plasma core to ≈7.8% at the reactor walls. This is not a signature of Ar chemistry! Rather, it is a manifestation of mass-dependent thermodiffusion, also known as the Soret effect—the preferential diffusion of heavier species down a temperature gradient.[76,77] Hydrocarbon species in an excess of H_2 are subject to similar thermodiffusion effects, and so the total carbon mole fraction in the hot region will be lower than that in the input gas mixture.

The remaining panels in Figure 4 illustrate the conversion of CH_4, panel (f) into C_2H_2, panel (g), as the input gas mixture diffuses from the inlet (at the top corner of the images) into regions of higher T_{gas} and [H] closer to the substrate. The $X(C_2H_2)$ distribution throughout the whole

reactor is much flatter than that of $X(CH_4)$ but, when plotted in terms of $[C_2H_2]$ (Figure 4(h)), we are again reminded of the way the total number density varies with T_{gas}. As with Ar, the highest number densities of stable species like C_2H_2 (and CH_4) in these MW activated H/C plasmas are found at the (cold) periphery of the reactor. This has major implications for line-of-sight absorption measurements of such stable species, and the interpretation of such measurements, since the measured absorbances will typically be dominated by molecules at the end of the viewing column, far from any growing diamond surface.[46]

We find it helpful to picture the reactor volume in terms of three nested regions.[67] Each supports H-shifting reactions within and between the CH_x and C_2H_y families illustrated in Figure 2, but with rates that are sensitive to T_{gas}, so that the dominant species vary between them. The outer region having T_{gas} < 1500 K (labelled **C** in Figure 4(g)) is characterised by net $C_2H_y \rightarrow CH_x$ conversion, and our model returns $[CH_4] > [C_2H_2]$ throughout this region. In contrast, region **B** (1500 < T_{gas} < 2500 K), the annular shell around the central plasma region, is characterized by net production of C_2H_y species, reflecting the effect of increased T_{gas} on the $CH_x \rightarrow C_2H_y$ inter-conversion rates. $[C_2H_2] > [CH_4]$ throughout region **B** (including close the substrate surface), as well as in region **A** (T_{gas} >2500 K), such that C_2H_2 accounts for >97% of all the carbon in the plasma proper under our base conditions. Diffusive mixing between regions **C** and **B** is important in maintaining the balance between them, and the extent of gas processing in these regions ensures that this result holds irrespective of the choice of input hydrocarbon. The rates of the $CH_x \leftrightarrow C_2H_y$ inter-conversion reactions within regions **B** and **A** are sufficiently high to ensure local equilibration and the CH_x / C_2H_y balance in the plasma region is simply determined by the local T_{gas} and $X(H)$.[67]

Experimental validation of these conclusions is provided by Figure 5, which shows two sets of *z*-resolved absolute column density profiles for C_2(a, v=0) and CH(X, v=0) radicals, and for electronically excited H(n = 2) atoms, measured (by CRDS) under process conditions that differ in just one important detail.[44,78] The data shown by the solid symbols were obtained for the same p, P and gas mixture as used for the model outputs displayed in Figure 4 (*i.e.* a CH_4 flow rate, $F(CH_4)$ = 25 sccm), while those given as open symbols were recorded using C_2H_2 as the carbon source gas, at $F(C_2H_2)$ = 12.5 sccm, with a compensatory increase in $F(H_2)$ to ensure the same input carbon fraction and total flow rate. The two sets of column densities are indistinguishable, reinforcing the conclusion that the plasma chemistry and composition in the growth-relevant volume is insensitive to the chosen carbon source. The modelling reveals no significant net sources or sinks of gas-phase carbon-containing species in region **A**. Near the

substrate, the sharp decline in T_{gas} strongly compresses regions **B** and **C**, but these thin zones are predicted to support analogous net chemical transformations to those recognized at large *r* and *z*. However, the steep concentration and temperature gradients encourage transport by diffusion (including thermodiffusion), and so enhance species mixing in the near-substrate volume.

The absorption measurements (Figure 5) returned maximum column densities for CH and C_2 radicals at $z \sim 10$ mm, and the modelling (i) confirms that both species are concentrated in the hot region and (ii) reproduces the measured column densities.[44] Calculated number density distributions for C_2, C_2H, CH and CH_3 radicals in the same base H/C/Ar plasma as that featured in Figure 4 are shown in the form of 2-D(*r*, *z*) false-colour plots in Figure 6. Consistent with Figure 2, which suggested that the formation of C_2 and C_2H is favoured by high [H] and high T_{gas}, Figures 6(a) and 6(b) show these species most tightly concentrated within the plasma core. The [CH] distribution, Figure 6(c), is more extensive; the calculated [CH_3] distribution, Figure 6(d), extends further still and that for [CH_2] (not shown) is intermediate between these two.[44] Indeed, the CH_3 number density distribution is predicted to maximise in a thin shell corresponding to a narrow range of [H] and T_{gas} at the periphery of the hot region—a point to which we return below.

The chemistry by which carbon-containing gas-phase radicals are transformed into carbon atoms incorporated in a growing diamond lattice would constitute another excellent topic for a Feature Article, but can be addressed here only in passing. The 'standard model' of diamond CVD includes several key elements.[26,30,79-82] First, the diamond surface is stabilized and its graphitic rearrangement is suppressed by terminating H atoms, and T_{sub} is sufficiently below the Debye temperature of diamond to prevent spontaneous bulk rearrangement. Second, the gaseous activation process converts H_2 to H atoms, which react with the carbon source and create a complex mixture of species including reactive hydrocarbon radicals—the focus of this paper. Third, these gas phase H atoms also abstract hydrogen from surface C–H bonds, thereby creating surface radical sites that occasionally react with a gas-phase radical to yield a chemisorbed CH_x moiety. Much more frequently, however, the surface radical sites are simply refilled by recombining with another H atom incident upon them from the gas phase. This continual turnover of the surface termination drives the surface chemistry to dehydrogenate adsorbed carbon species and facilitates (limited) migration of the adsorbates, so enabling incorporation of their carbon atoms into the lattice. Finally, the H atoms react with any *sp* or sp^2-bonded carbon on the surface, thereby either converting these sites to sp^3 or etching non-

diamond material back into the gas phase. Most diamond growth models now consider CH_3 to be the principal species that adds to a surface radical site in order to be incorporated into the growing crystal.[79,83-86] Such an assumption is very much encouraged by plasma-chemical modelling such as ours, with our specified base conditions leading to $[CH_3] \sim 10^{14}$ cm^{-3} in the near-surface region, as can be seen in Figure 6(d). This value is both two orders of magnitude larger than that of any other CH_x species and relatively constant across the substrate surface.[44,67]

In many regards, understanding MW plasma-activated H/C gas mixtures under conditions relevant to diamond CVD is a solved problem. Combined experimental and modelling approaches such as ours have provided full descriptions of the plasma processing, the spatially resolved variation of T_{gas} and the gas-phase composition, the influence of process conditions (P, p, carbon input fraction, etc.), and at least some of the links between the gas-phase and gas–surface chemistry. The same techniques can, of course, be applied to non-hydrocarbon species in the same environment, and we proceed to briefly summarise the results of similar recent studies of various H/C/dopant plasmas.

2.3 H/C/B plasmas

Semiconducting diamond has long been recognised as a potentially important material for high power and high temperature electronic applications. Reliable growth of high quality *n*-type diamond remains challenging, but growth of *p*-type material with good conductivity is now routinely achieved by incorporating boron into the diamond lattice during CVD.[87-89] B-doped CVD diamond can be conveniently prepared by adding suitable trace amounts of diborane (diluted in H_2) into the source gas mixture, and the recent literature contains several reports of experimental (OES, CRDS and tunable infrared absorption spectroscopy) and modelling studies of MW activated $B_2H_6/H_2/(Ar)$ [70,90-93] and $B_2H_6/CH_4/H_2/(Ar)$ [54,92-95] gas mixtures.

Small B_2H_6 additions (even at the tens to hundreds of parts per million level) have negligible effect on the established H/C/(Ar) plasma chemistry. Our measurements are all consistent with a model wherein input B_2H_6 undergoes thermal dissociation on approaching the hotter plasma regions. The resulting BH_3 radicals participate in a sequence of H-shifting reactions, leading to a distribution of BH_x (x = 0-3) species. Much of the input boron is deduced to be stored in reservoir species like CH_2CHBH_2 and $CH_3CH_2BH_2$ (and, in the presence of trace air impurity, HBO, H_2BO and H_3COBH_2) in cooler regions of the reactor, but modelling the reactions involved in the formation and destruction of such species is hampered by a lack of relevant thermodynamic and kinetic information.[54]

Figure 7 shows 2-D (r, z) number density distributions for the various BH_x species calculated for an H/C/B/Ar plasma operating under the same base conditions of p, P, CH_4, H_2 and Ar flow rates as in Figures 4 and 6 with, additionally, $F(B_2H_6)$ = 0.009 sccm and an air impurity that was assumed to contribute $F(O_2)$ = 0.006 sccm. The respective [BH_x] profiles reflect the complex balance of diffusional transfers and inter-conversions between the various families of B-containing species in the different local environments (T_{gas}, [H], [H_2O], [CH_x], [C_2H_y], *etc*) within the reactor volume. Irrespective of the trace air impurity assumed, however, the calculations predict that atomic boron will be the most abundant gas phase BH_x species near the substrate surface during diamond CVD, and our gas-surface modelling has focussed on elementary reaction sequences whereby B atoms and BH radicals can add to radical sites and/or insert into C–H bonds on the growing diamond surface.[96,97]

2.4 H/C/N plasmas

Nitrogen is an *n*-type dopant of diamond, but is a deep donor;[98] N-doped diamond has not yet proved suitable for many of its envisioned electronic applications. Given that nitrogen constitutes 80% of any air impurity, it is impossible to grow CVD diamond that is completely N-free. Fortunately, several studies have demonstrated that the presence of (suitably small amounts of) nitrogen in the standard H/C gas mixture actually results in an increased CVD diamond growth rate.[99-108] The presence of nitrogen also affects the morphology of the CVD diamond, encouraging formation of {100}- rather than {111}-facetted films.[109,110] Too much nitrogen in the gas mixture, however, results in inferior material, with small, poorly-oriented surface facets and a higher sp^2 fraction.[99,111] Why nitrogen causes these effects is still far from fully understood. Indeed, prior to our recent combined experimental (OES and CRDS) and modelling studies of MW activated H/N [112] and H/C/N [71] gas mixtures, even the identities of the more abundant N-containing species near the growing surface during diamond CVD was unclear.

As in the case H/C/B plasmas, small N_2 additions have little impact on the established H/C plasma chemistry. Comparative diagnoses of MW activated N_2/H_2 and NH_3/H_2 plasmas reveal that both direct EI dissociation of N_2 and EI induced formation of metastable $N_2(A^3\Sigma^+_u)$ molecules (which can react with H atoms), together with subsequent H-shifting reactions, serve to convert some of the strongly bound N_2 molecules into reactive NH_x (x = 0-3) species.[71] Reactions of CH radicals (and C atoms) with N_2 are further N atom sources in the case of H/C/N plasmas, wherein reactions between NH_x (x = 0-3) and CH_x (x = 0-3) radicals then provide the route to forming HCN (which, like C_2H_2, is a stable species in the hot region).[57,61]

Notwithstanding, N_2 still constitutes ~99.5% of the total nitrogen in the core of a MW activated H/C/N plasma operating under our base conditions of *p* and *P*. Less than 0.25% of the input N_2 is converted to HCN and the relative abundances of N-containing species that might plausibly be considered reactive at the growing diamond surface (*e.g.* N atoms, NH, NH_2 and CN radicals) are all two or more orders of magnitude lower still. Of these, as Figure 8 shows, the near-surface value of [N] for the employed base flow rates ($F(N_2)$ = 3 sccm, $F(CH_4)$ = 20 sccm) is higher than that of [NH] (or [NH_2]), and almost an order of magnitude higher than that of [CN]. Changing the N/C ratio in the input gas mixture under base conditions causes a proportional change in the near-surface [N]/[CH_3] ratio, but has little effect on the [N]/[NH]/[CN] ratios just above the growing surface. The near surface [N]/[CH_3] ratio is consistently much smaller than the N_2/CH_4 ratio in the input gas mixture, re-emphasising the stability of N_2 under the prevailing process conditions. Increasing *p* or *P* promotes N_2 dissociation, and so raises the near surface [N]/[CH_3] and [CN]/[CH_3] ratios for any given N input fraction.[71]

Complementary gas-surface modelling has built on these findings and identified elementary reaction sequences by which N atoms and both NH and CN radicals could incorporate at a (100):H 2×1 reconstructed diamond surface.[113] As noted above, N atoms are more abundant close to the growing diamond surface but, given the efficiency of the H-shifting reactions, NH is viewed as the more probable migrating species which can incorporate at a single-atom step edge on the surface. Subsequent H abstraction (by reaction with a gas phase H atom) and further C additions could then lead to a sub-surface N atom – such as has been proposed as a possible route to catalysing diamond growth.[114] N incorporation via CN addition on the C(100):H 2×1 diamond surface is considered less probable for several reasons,[113] but remains an intriguing prospect as such a mechanism would add two heavy atoms, and leave the N atom sitting proud of the current growth layer. This could serve as a nucleation site for next layer growth and, given that such nucleation is generally perceived to be the rate limiting step in diamond growth, enhance the material growth rate.

2.5 H/C/O plasmas

Most CVD diamond is now grown from CH_4/H_2 gas mixtures, but early studies explored a range of H/C/O source gas mixtures – from the perspectives of both the gas phase chemistry / composition (as deduced by OES or mass spectrometry), and the rate / "quality" of the diamond growth.[115-122] These early studies demonstrated that successful diamond growth was restricted

to a limited range of input gas compositions and suggested that H/C/O plasmas offered a route to diamond growth at lower T_{sub} than with the traditional H/C gas mixtures.

In contrast to the foregoing H/C/B and H/C/N gas mixtures, the H/C/O plasmas that support diamond CVD cannot be viewed as lightly perturbed variants of the basic MW activated H/C gas mixture. The O is not introduced as a trace dopant. Rather, diamond growth requires that the elemental O content (X_{elem}(O)) in the input gas mixture almost matches the elemental C content (X_{elem}(C)). Following Bachmann,[123] it will prove helpful to characterise the input source gas mixture using the $X_{C/\Sigma}$ notation, where

$$X_{C/\Sigma} = X_{elem}(C) / \{X_{elem}(C) + X_{elem}(O)\}. \quad (5)$$

Again, a combination of *in situ* OES and CRDS diagnoses and 2-D modelling of MW activated $CH_4/CO_2/H_2$ plasmas has provided a rationale for the various observations.[56,72] Most attention was focussed on CH_4/CO_2 mixtures, with H_2 added as 30% of the total input gas flow to help stabilise the plasma. $X_{C/\Sigma} = 0.5$ in the case that $F(CH_4) = F(CO_2)$. The modelling identifies CO and H_2 as the main species in the plasma core. The lower thermal conductivity of such a mixture (*cf*. the H_2-rich plasmas used in most diamond CVD) explains the finding that $CH_4/CO_2/H_2$ plasmas can yield similar maximum T_{gas} values and diamond growth rates at lower input powers than traditional CH_4/H_2 plasmas (albeit in a smaller plasma volume and over a smaller substrate surface area).

Experiment and modelling both show a switch in the plasma chemistry and composition on changing from O-rich ($X_{C/\Sigma} < 0.5$) to C-rich ($X_{C/\Sigma} > 0.5$) gas mixtures.[56] The 2-D calculations predict significant C_2H_2 and H_2O production in the annular shell around the plasma region, leading to steady-state mole fractions of several percent in each case, which act as sources of, respectively, reactive carbon and oxygen in the hot region. Figure 9 shows how the calculated 2-D(r, z) spatial distribution of $X(C_2H_2)$ evolves as the mixture is tuned from O-rich (Figure 9(a), $X_{C/\Sigma} = 0.47$) to C-rich (Figure 9(c), $X_{C/\Sigma} = 0.54$). At $X_{C/\Sigma} = 0.47$, the excess of oxygen-containing radicals (O, OH) in the hot region converts hydrocarbon species to CO, leaving the plasma region deficient in carbon-containing species and X(CH), $X(C_2)$, *etc*. concentrated in an annular shell around the plasma core. This deficiency is rectified by raising $X_{C/\Sigma}$ above 0.5, whereupon the oxygen-containing radicals are no longer in excess and $X(CH_x)$, $X(C_2)$, *etc*. build up in the hot region.[56] As in H/C plasmas, the CH_3 radical density is concentrated in a mid-temperature region around the plasma core. Though not immediately obvious from the false color $X(CH_3)$ plots shown in Figure 9, $[CH_3]$ close above the substrate surface increases by

more than two orders of magnitude on moving across the $X_{C/\Sigma} = 0.5$ boundary. (The calculated $[CH_3](r = 0, z = 0.5$ mm) values for the process conditions specified in the caption to Figure 9 are 7.4×10^{10}, 2.5×10^{13} and 5.1×10^{13} cm^{-3} for $X_{C/\Sigma} = 0.47$, 0.50 and 0.54, respectively). The calculated spatial distributions of X(O) and X(OH) show the reverse behavior to X(CH), $X(C_2)$, *etc*.[56] Both of these O-containing species are depleted in the hot region by reaction with hydrocarbon species to form CO at $X_{C/\Sigma} = 0.54$, but both distributions 'fill in' as $X_{C/\Sigma}$ is reduced below 0.5. As in the case of the H/C/N plasmas, the 2-D modelling also revealed important roles for metastable species ($CO(a^3\Pi)$ molecules in this case, formed by EI excitation of ground state CO molecules) in radical (H, C, OH) production and in transforming absorbed MW power into gas heating.[56]

Such behavior accounts for the narrow compositional process window for successful diamond growth from $CH_4/CO_2/H_2$ gas mixtures. $X_{C/\Sigma}$ must be ≥0.5 in order that the density of active carbon species in the near substrate region exceeds that of O and OH. CH_3 radicals are identified as the most abundant CH_x (x = 0-3) species near the growing diamond surface within the range used for diamond growth ($X_{C/\Sigma}$ ~0.5-0.54). This, together with the findings that the maximum T_{gas} (~2800-3000 K) and X(H) (~5-10%) values in the plasma core are both comparable to those found in MW activated H/C plasmas, points to similar CH_3 radical based diamond growth mechanisms in both H/C and H/C/O plasmas. We also note a point of distinction, however. In contrast to the H/C plasmas, the chemistry and composition prevailing in H/C/O plasmas can be source gas dependent. Specifically, the H:C:O ratios in the base $CH_4/CO_2/H_2$ ($X_{C/\Sigma}$ = 0.5) mixture for the simulations reported in Figure 9(b) can also be achieved using a 41.2% CO/58.8% H_2 gas mixture but, in this particular case, the stability of CO ensures differences in both the gas activation and the ensuing plasma chemistry and composition.[56]

2.6 Anions in CH_4/H_2 plasmas.

The preceding discussions of the MW activated gas mixtures have all been couched in terms of (low concentrations of) electrons and the counter-cations needed to ensure overall charge neutrality in the plasma region, along with orders of magnitude higher densities of neutral species. Such a narrative was consistent with all published works until the start of this year, when spatially resolved optical emission imaging studies revealed a hitherto unrecognised (in the context of MW activated CH_4/H_2 plasmas) emission attributable to electronically excited C_2^- anions in the same spectral region as the commonly observed C_2 Swan bands.[124] Various

possible formation mechanisms were considered, only one of which – dissociative electron attachment (DEA) to C_2H radicals (recall Figure 6(b)) resulting in direct formation of the observed excited C_2^- anions, balanced by the inverse associative detachment process – was consistent with the observed spatial distributions and the measured variations in emission intensity with changes in *p*, *P* and the H/C/(Ar) ratio in the input gas mixture. Similar 2-D plasma-chemical modelling predicts that DEA to C_2H_2 must be a yet more important source of ground state C_2H^- anions in such plasmas, and that DEA to HCN will be an efficient route to forming CN^- anions in H/C/N plasmas. The predicted total anion densities are never >0.1% of the cation density under any conditions investigated, but this recent study serves to remind us that, despite the substantial advances of the past decade, there is still room for further improvements in our understanding of the MW activated gas mixtures employed in diamond CVD.

3. A Prospective View

The last decade has witnessed huge strides in our knowledge and understanding of the gas phase chemistry prevailing in MW activated H/C plasmas, and in H/C plasmas containing added boron, nitrogen and oxygen containing species, and it is appropriate to conclude by reflecting on remaining challenges. Diamond growth occurs at the gas-surface interface, and it is fair to note that there is still much work required to determine the extent of gas processing in the boundary layer immediately above the growing surface, and in the larger scale simulation of diamond growth from the gas phase.[125-127]

Another valid question is the extent to which all the foregoing plasma chemical insights could be used to enhance the efficiency of the diamond CVD process. Efficiency can be assessed in several ways. Polycrystalline diamond growth rates from an H/C plasma operating at our base conditions are typically ~2 μm hr^{-1}. Given a 30 mm substrate diameter, this equates to ~5 mg of diamond per hour, equal to just 0.6% of the carbon delivered in the source gas during that time. The energy consumed in this time is 5.4 MJ. As first proposed by Goodwin,[128] and discussed earlier in this Feature Article, key factors for successful diamond growth using a medium pressure MW CVD reactor are the H atom and CH_3 radical densities at the growing diamond surface and an appropriate T_{sub}. [H] in the bulk of the plasma can be increased by operating at higher power densities *Q* (and thus higher maximum T_{gas}), which can be achieved by complementary increases in *p* and *P*.[129] The transport of H atoms from the plasma core is diffusion limited, so the near surface H atom number density, $[H]_{ns}$, is assumed to scale

similarly with p and P.[130] Simply increasing $[H]_{ns}$ will be counter-productive, however, if its effect is primarily to increase the rate of diamond surface etching.

Increased growth rates also require an appropriate increase in $[CH_3]_{ns}$ but, as we saw in Figure 6, the H-shifting equilibria between the various CH_x species are very sensitive to the local T_{gas} and [H] values. $[CH_3]$ is favoured by intermediate T_{gas} values in the range 1500-2100 K and tends to concentrate in an annular shell around the plasma core, which includes a narrow sheath in the boundary layer just above the substrate. Higher growth rates at higher Q have been achieved by increasing $F(CH_4)$ also. For example, Derkaoui *et al*. have reported a ~10-fold increase in the rate of diamond CVD (defined in μm hr^{-1}) on a small ($3 \times 3 \times 1.5$ mm^3) single crystal diamond substrate by combined increases in p (from 110 to 285 Torr), P (from 2.5 to 3 kW) and $F(CH_4)$ (from 4 % to 7 % of the input gas mixture).[129] This increase in growth rate is accompanied by a ~2-fold boost in carbon utilisation efficiency and a ~8-fold improvement in energy efficiency. There is a limit to how far such 'brute force' strategies can be pursued, however, as sooty inclusions were clearly evident in the CVD-grown diamond once CH_4 constituted more than 10% of the total input gas mixture.[129] Thus these workers conclude that simply increasing the amount of CH_4 in the input source gas is likely to be of limited value as a means of boosting the growth rate, but injecting additional CH_4 directly into the boundary layer of a pre-existing plasma might be more fruitful. As noted in section 2.4, judicious addition of traces of N_2 to the H/C process gas mixture offers another route to increasing the diamond growth rate without compromising the quality of the deposited material.[106,107]

Finally, we briefly consider the issue of reactor design. From all the above, it should be clear that there must be an optimum set of $[H]_{ns}$, $[CH_3]_{ns}$ and T_{sub} values for optimum growth of CVD diamond – as judged by growth rate or by material quality. But few, if any, reactors are designed to allow independent optimisation of these parameters. $[H]_{ns}$ is determined by Q, T_{gas}, *etc*., $[CH_3]_{ns}$ depends on the input $X(CH_4)$ and the local T_{gas} and [H], and T_{sub} is affected by the proximity of the hot plasma and by $[H]_{ns}$ (since the recombination of H atoms on its surface is a significant source of substrate heating [55]). T_{sub} can be controlled and optimised in a purpose-designed reactor by inclusion of an appropriate secondary heating/cooling unit. Optimising both $[H]_{ns}$ and $[CH_3]_{ns}$ at the growing diamond surface, simultaneously, is nigh on impossible, however, and the most promising approach at this time appears to involve designing the MW reactor with sufficient flexibility that the exact position of the substrate can be fine-tuned during operation so as to sample the best compromise $[H]_{ns}$ and $[CH_3]_{ns}$ values.[131,132]

4. Acknowledgements

The Bristol authors acknowledge financial support from Engineering and Physical Sciences Research Council (EPSRC) grant no. EP/K018388/1, the EPSRC Centre for Doctoral Training in Diamond Science and Technology (EP/L015315/1) and from Element Six Ltd. The authors are also grateful for the many and varied contributions from past and present colleagues Professor Paul May and Drs Colin Western, Jie Ma, James Richley, Mark Kelly and James Smith. The work was performed within the Cooperation in Science and Technology Agreement between Lomonosov Moscow State University, Skobeltsyn Institute of Nuclear Physics, and the University of Bristol. No new data were created specifically for this study.

Mike Ashfold obtained his PhD from the University of Birmingham in 1978. After postdoctoral research at the University of Oxford, he was appointed as a Lecturer at the University of Bristol, where he was promoted to a Chair in Physical Chemistry in 1992. He was elected to the Fellowship of the Royal Society in 2009. His research interests include plasma diagnosis (particularly in the context of diamond CVD), molecular photophysics and spectroscopy.

Ed Mahoney gained an MPhys degree in Physics from the University of Warwick in 2014 and was selected into the Diamond Science and Technology Centre for Doctoral Training, through which he is now working towards a PhD degree focussed on optical diagnosis of MW activated plasmas relevant to diamond CVD.

Sohail Mushtaq obtained his MPhil degree from the Government College University Lahore, Pakistan, and his PhD from Imperial College London (2011). He held a Pillow Postdoctoral Research Fellowship at London Metropolitan University, specialising in optical emission and mass spectroscopy of analytical glow discharges, before joining the Bristol Diamond Group in early 2017.

Ben Truscott obtained his MChem and PhD degrees from the University of Bristol in 2008 and 2013, then led projects spanning laser induced plasmas, high pressure microdischarges and plasma diagnostics for diamond CVD in Bristol as a Postdoctoral Fellow. He was appointed as a Research Scientist with Element Six Ltd. in late 2016.

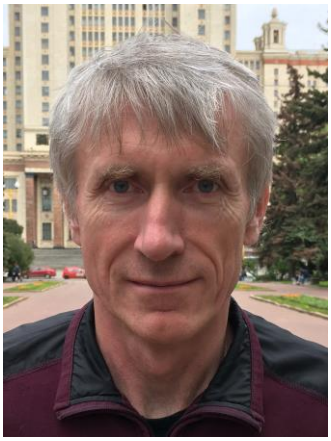

Yuri Mankelevich obtained his PhD in 1989 at the Moscow Institute of Physics and Technology and the Keldysh Institute of Applied Mathematics, and has since held Scientist, Senior Scientist and (since 2010) Leading Scientist positions in the Microelectronics Department of the Skobel'tsyn Institute of Nuclear Physics at the Lomonosov Moscow State University (LMSU). He gained his Doctor of Physical-Mathematical Sciences degree in 2014 at LMSU. His research interests include modelling diamond CVD processes in hot filament, DC, DC arc-jet and MW plasma activated CVD reactors, and plasma-surface interactions (especially in the context of etching and damage mechanisms in microelectronics processing).

Figure Captions.

Figure 1

Cross-section and tilt view scanning electron microscope (SEM) images illustrating (a) micro- and (b) nanocrystalline morphologies of CVD diamond films grown on Si substrates.

Figure 2

H-shifting reaction sequences that drive the conversion of CH_4 to C_2H_2 and other CH_x ($x \leq 3$) and C_2H_y ($y \leq 6$) species in regions of high [H] and high T_{gas}.

Figure 3

MW plasma reactor in operation (right) along with a cross-section (left) illustrating selected features of the reactor and the probe laser beam path.

Figure 4

Calculated 2-D(r, z) distributions of (a) n_e, (b) T_{gas}, (c) [H], (d) [H_2], (e) X(Ar), (f) X(CH_4), (g) X(C_2H_2) and (h) [C_2H_2] for a MW activated gas mixture comprising F(CH_4) = 25 sccm, F(Ar) = 40 sccm, F(H_2) = 500 sccm, operating at p = 150 Torr and with P = 1.5 kW. The model assumes cylindrical symmetry, a reactor radius, r = 6 cm and height, h = 6.2 cm, and a substrate diameter of 3 cm.

Figure 5

Comparison of C_2(a, v=0) and CH(X, v=0) radical (left hand scale) and H(n=2) atom (right hand scale) column densities measured by CRDS spectroscopy as a function of height (z) above the substrate surface in the same MW CVD reactor, operating at the same p (150 Torr) and P (1.5 kW), using the following gas mixtures: (i) F(CH_4) = 25 sccm, F(Ar) = 40 sccm, F(H_2) = 500 sccm and (ii) F(C_2H_2) = 12.5 sccm, F(Ar) = 40 sccm, F(H_2) = 512.5 sccm (filled and open symbols, respectively).

Figure 6

Calculated 2-D(r, z) distributions of (a) [C_2(a)], (b) [C_2H], (c) [CH] and (d) [CH_3] for the same reactor and operating conditions as in Figure 4.

Figure 7

Calculated 2-D(r, z) distributions of (a) [B], (b) [BH], (c) [BH_2] and (d) [BH_3] in a MW activated gas mixture comprising F(CH_4) = 25 sccm, F(Ar) = 40 sccm, F(H_2) = 500 sccm, F(B_2H_6) = 0.009 sccm and F(O_2) = 0.006 sccm. All other details are as in Figure 4.

Figure 8

Calculated 2-D(r, z) distributions of (a) [N], (b) [NH], (c) [NH_3] and (d) [CN] in a MW activated gas mixture comprising $F(CH_4)$ = 20 sccm, $F(N_2)$ = 3 sccm and $F(H_2)$ = 477 sccm, with all other details as in Figure 4.

Figure 9

Calculated 2-D(r, z) mole fraction distributions $X(CH_3)$ and $X(C_2H_2)$ in a MW activated $CH_4/CO_2/H_2$ gas mixture comprising $F(CH_4) = 350X_{C/\Sigma}$ sccm, $F(CO_2) = 350(1 - X_{C/\Sigma})$ sccm and $F(H_2)$ = 150 sccm, with p = 150 Torr, P = 1 kW and $X_{C/\Sigma}$ = (a) 0.47, (b) 0.5 and (c) 0.54. The reactor dimensions for the modelling are the same as in Figure 4.

Figure 1

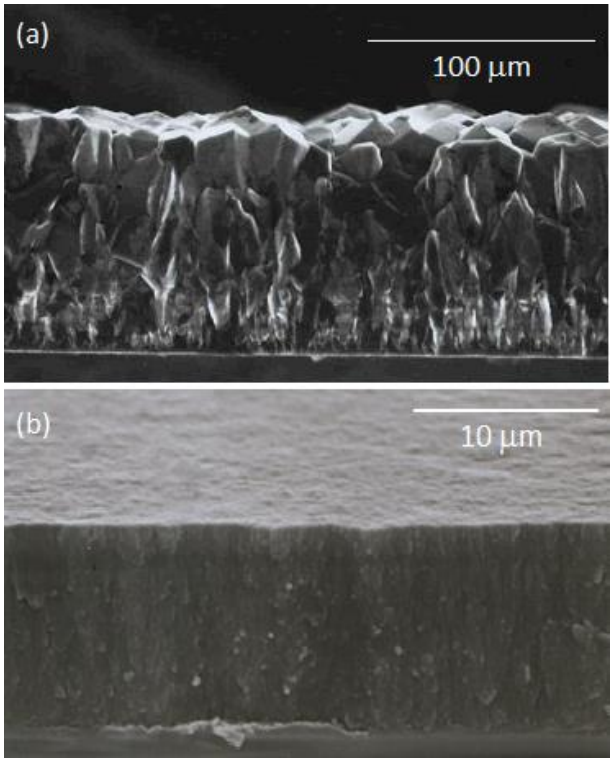

Figure 2

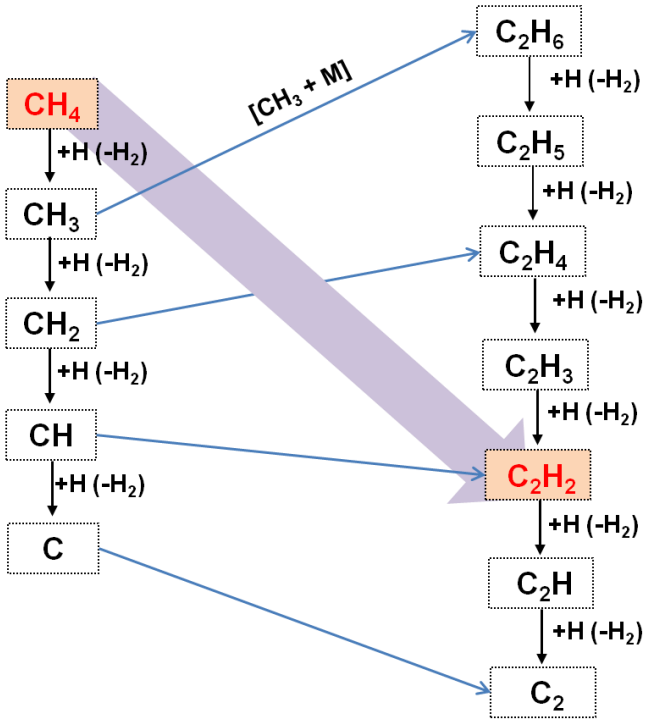
CH4
+H (-H2)
CH3
+H (-H2)
CH2
+H (-H2)
CH
+H (-H2)
C
[CH3 + M]
C2H6
+H (-H2)
C2H5
+H (-H2)
C2H4
+H (-H2)
C2H3
+H (-H2)
C2H2
+H (-H2)
C2H
+H (-H2)
C2

Figure 3

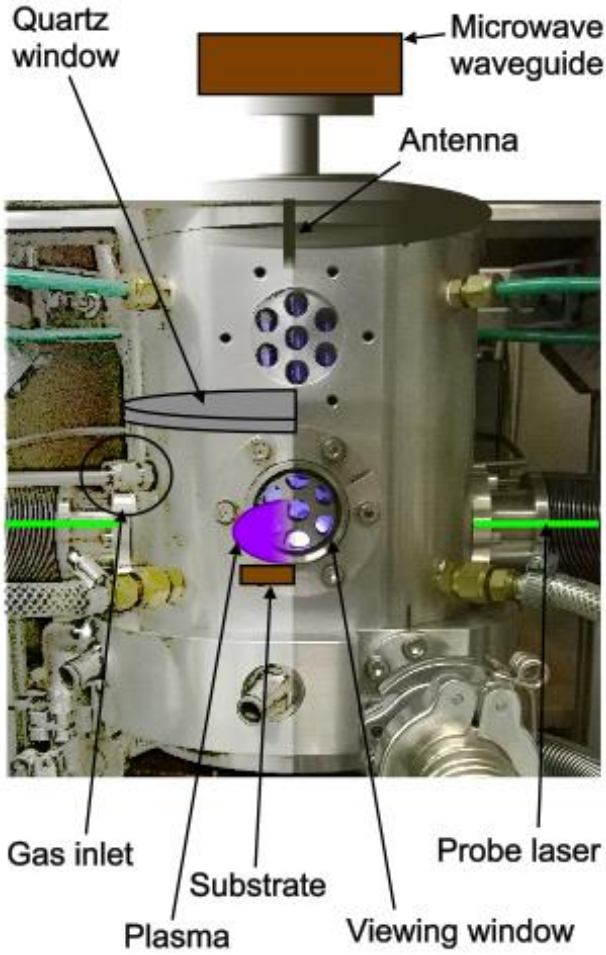
Quartz window
Microwave waveguide
Antenna
Gas inlet
Substrate
Plasma
Viewing window
Probe laser

Figure 4

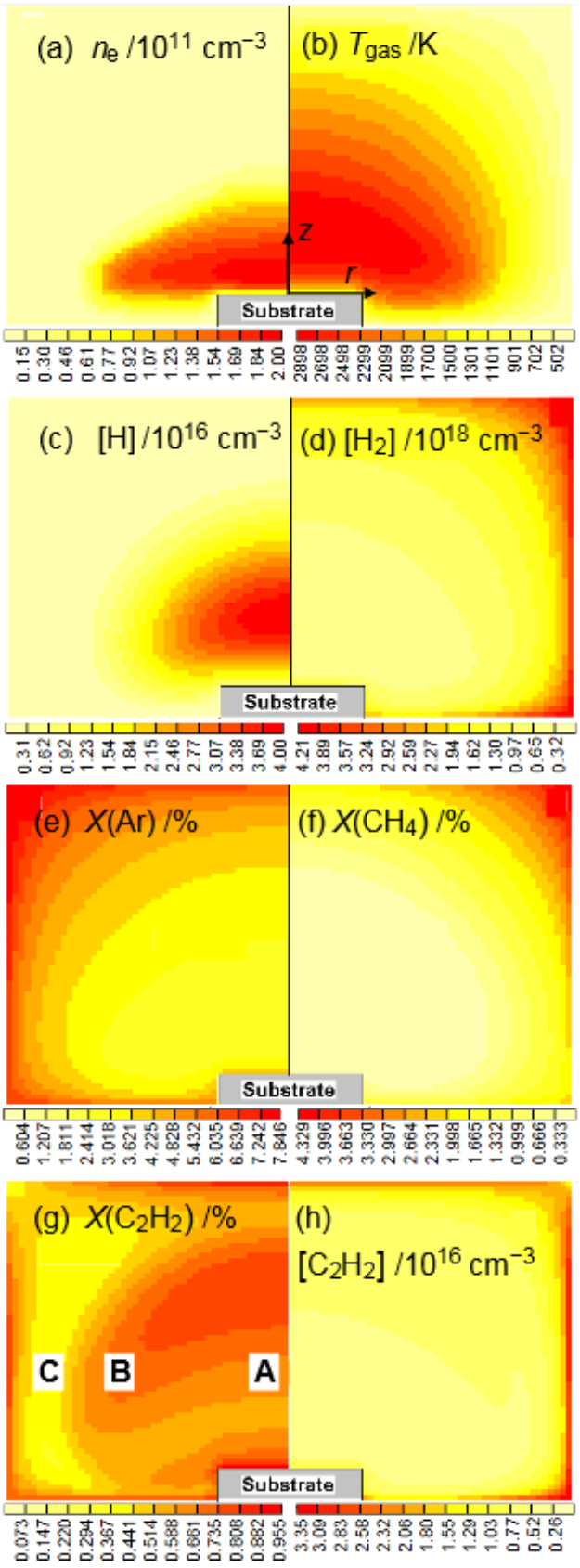
(a) n_e /10^{11} cm^{-3}
(b) T_{gas} /K
z
r
Substrate
0.15 0.30 0.46 0.61 0.77 0.92 1.07 1.23 1.38 1.54 1.69 1.84 2.00
2898 2698 2498 2299 2099 1899 1700 1500 1301 1101 901 702 502
(c) [H] /10^{16} cm^{-3}
(d) [H_2] /10^{18} cm^{-3}
Substrate
0.31 0.62 0.92 1.23 1.54 1.84 2.15 2.46 2.77 3.07 3.38 3.69 4.00
4.21 3.89 3.57 3.24 2.92 2.59 2.27 1.94 1.62 1.30 0.97 0.65 0.32
(e) X(Ar) /%
(f) X(CH_4) /%
Substrate
0.604 1.207 1.811 2.414 3.018 3.621 4.225 4.828 5.432 6.035 6.639 7.242 7.846
4.329 3.996 3.663 3.330 2.997 2.664 2.331 1.998 1.665 1.332 0.999 0.666 0.333
(g) X(C_2H_2) /%
(h)
[C_2H_2] /10^{16} cm^{-3}
C
B
A
Substrate
0.073 0.147 0.220 0.294 0.367 0.441 0.514 0.588 0.661 0.735 0.808 0.882 0.955
3.35 3.09 2.83 2.58 2.32 2.06 1.80 1.55 1.29 1.03 0.77 0.52 0.26

Figure 5

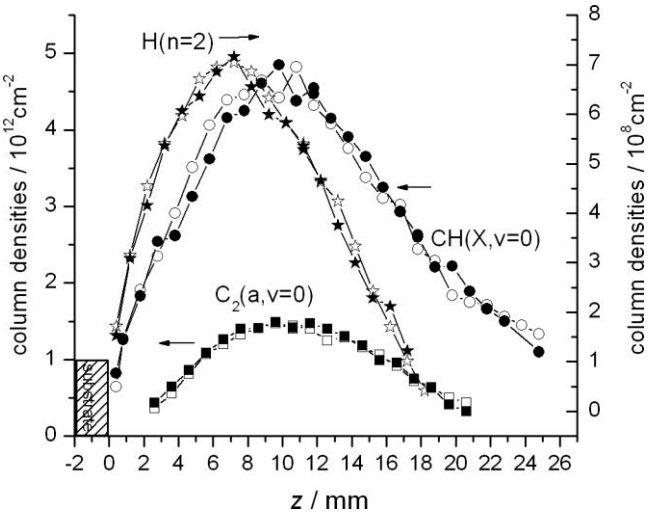
H(n=2)
CH(X,v=0)
C2(a,v=0)
absorb.
column densities / 10^12cm^-2
column densities / 10^8cm^-2
z / mm

Figure 6

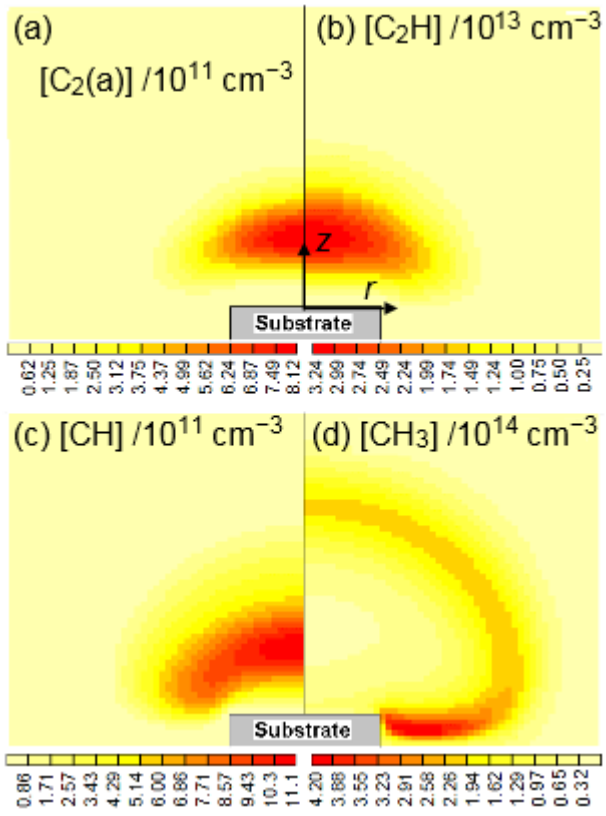
(a)
[C2(a)] /10^11 cm^-3
(b) [C2H] /10^13 cm^-3
z
r
Substrate
0.62 1.25 1.87 2.50 3.12 3.75 4.37 4.99 5.62 6.24 6.87 7.49 8.12
3.24 2.99 2.74 2.49 2.24 1.99 1.74 1.49 1.24 1.00 0.75 0.50 0.25
(c) [CH] /10^11 cm^-3
(d) [CH3] /10^14 cm^-3
Substrate
0.86 1.71 2.57 3.43 4.29 5.14 6.00 6.86 7.71 8.57 9.43 10.3 11.1
4.20 3.88 3.55 3.23 2.91 2.58 2.26 1.94 1.62 1.29 0.97 0.65 0.32

Figure 7

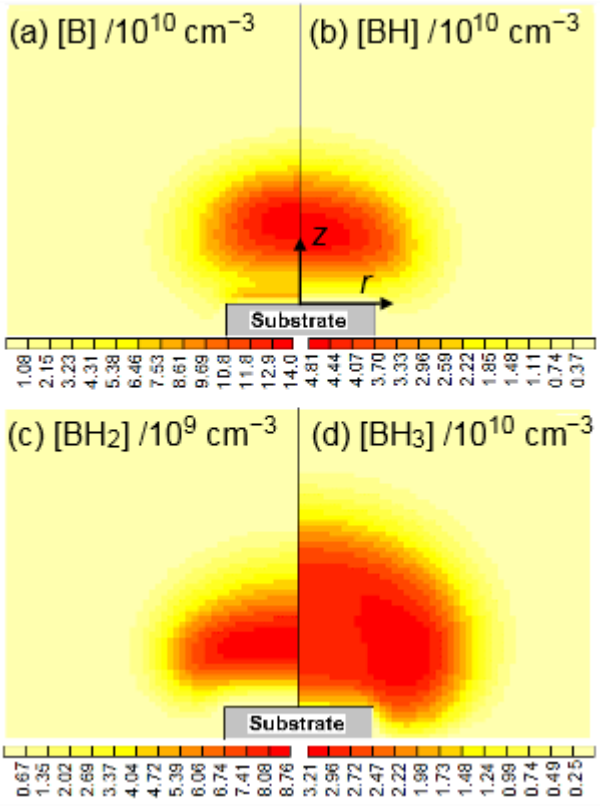
(a) [B] /10^10 cm^-3
(b) [BH] /10^10 cm^-3
z
r
Substrate
1.08 2.15 3.23 4.31 5.38 6.46 7.53 8.61 9.69 10.8 11.8 12.9 14.0
4.81 4.44 4.07 3.70 3.33 2.96 2.59 2.22 1.85 1.48 1.11 0.74 0.37
(c) [BH2] /10^9 cm^-3
(d) [BH3] /10^10 cm^-3
Substrate
0.67 1.35 2.02 2.69 3.37 4.04 4.72 5.39 6.06 6.74 7.41 8.08 8.76
3.21 2.96 2.72 2.47 2.22 1.98 1.73 1.48 1.24 0.99 0.74 0.49 0.25

Figure 8

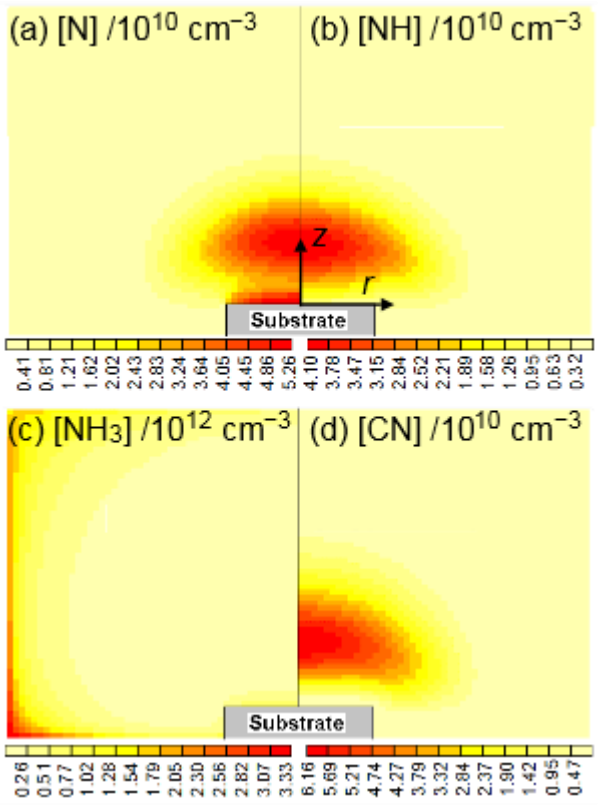
(a) [N] /10^10 cm^-3
(b) [NH] /10^10 cm^-3
z
r
Substrate
0.41 0.81 1.21 1.62 2.02 2.43 2.83 3.24 3.64 4.05 4.45 4.86 5.26 4.10 3.78 3.47 3.15 2.84 2.52 2.21 1.89 1.58 1.26 0.95 0.63 0.32
(c) [NH3] /10^12 cm^-3
(d) [CN] /10^10 cm^-3
Substrate
0.26 0.51 0.77 1.02 1.28 1.54 1.79 2.05 2.30 2.56 2.82 3.07 3.33 6.16 5.69 5.21 4.74 4.27 3.79 3.32 2.84 2.37 1.90 1.42 0.95 0.47

Figure 9

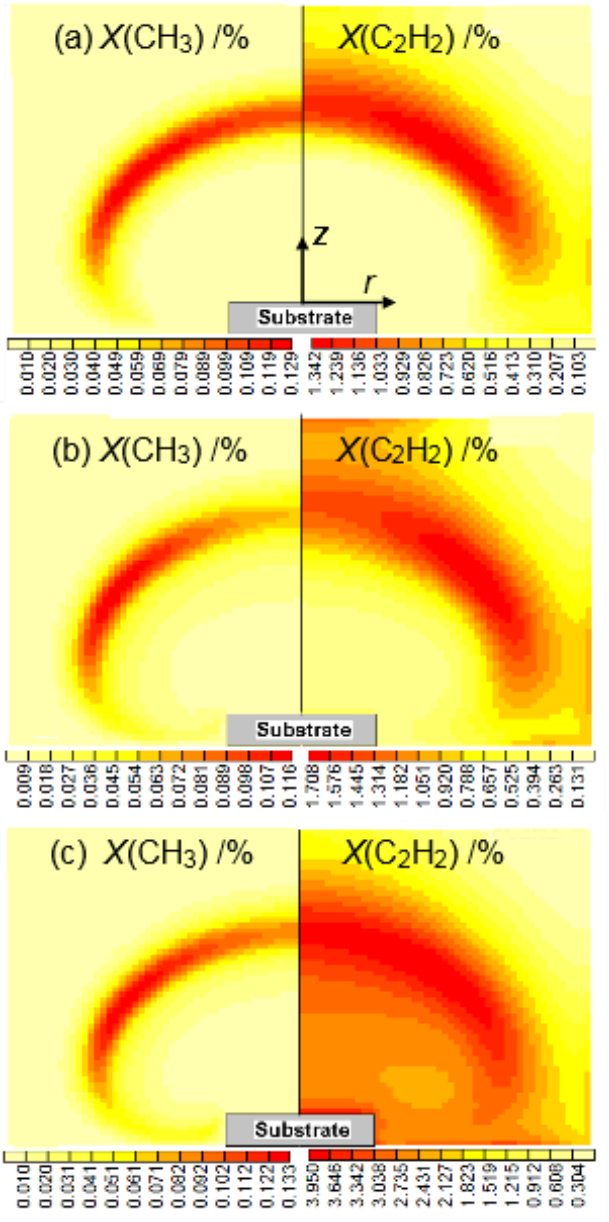
(a) X(CH3) /%
X(C2H2) /%
z
r
Substrate
0.010 0.020 0.030 0.040 0.049 0.059 0.069 0.079 0.089 0.099 0.109 0.119 0.129
1.342 1.239 1.136 1.033 0.929 0.826 0.723 0.620 0.516 0.413 0.310 0.207 0.103
(b) X(CH3) /%
X(C2H2) /%
Substrate
0.009 0.018 0.027 0.036 0.045 0.054 0.063 0.072 0.081 0.089 0.098 0.107 0.116
1.708 1.576 1.445 1.314 1.182 1.051 0.920 0.788 0.657 0.525 0.394 0.263 0.131
(c) X(CH3) /%
X(C2H2) /%
Substrate
0.010 0.020 0.031 0.041 0.051 0.061 0.071 0.082 0.092 0.102 0.112 0.122 0.133
3.950 3.646 3.342 3.038 2.735 2.431 2.127 1.823 1.519 1.215 0.912 0.608 0.304

Notes and References

[1] J.E. Field, *The Properties of Natural and Synthetic Diamond*. Academic Press, London, 1992.

[2] M.H. Nazare and A.J. Neves, *Properties, Growth and Applications of Diamond*. INSPEC, Institute of Engineers, London, 2001.

[3] G. Smith, *Journal of the South African Institute of Mining and Metallurgy* 2003, **103**, 529-534.

[4] M. Faraday, *A Course of Six Lectures on the Chemical History of a Candle* (ed. W. Crookes), 1861.

[5] Z.X. Su, W.Z. Zhou and Y. Zhang, *Chem. Comm.* 2011, **47**, 4700-4702.

[6] L.M. Hanssen, W.A. Carrington and J.E. Butler, *Mater. Letts*. 1988, **7**, 289-292.

[7] M.A. Cappelli and P.H. Paul, *J. Appl. Phys*. 1990, **67**, 2596-2602.

[8] K.V. Ravi, C.A. Koch, H.S. Hu and A. Joshi, *J. Mater. Res*. 1990, **5**, 2356-2366.

[9] B. Atakan, K. Lummer and K. Kohse-Höinghaus, *Phys. Chem. Chem. Phys*. 1999, **1**, 3151-3156.

[10] B.V. Spitsyn, L.L. Bouilov and B.V. Derjaguin, *J. Cryst. Growth* 1981, **52**, 219-226.

[11] S. Matsumoto, Y. Sato, M. Kamo and N. Setaka, *Jpn. J. Appl. Phys*. 1982, **21**, L183-L185.

[12] F.P. Bundy, H.T. Hall, H.M. Strong and R.H. Wentorf, *Nature* 1955, **176**, 51-55.

[13] V.M. Polushkin, A.T. Rakhimov, V.A. Samordov, N.V. Suetin and M.A. Timofeyev, *Diam. Rel. Mater*. 1994, **3**, 1385-1388.

[14] K.L. Menningen, M.A. Childs, H. Toyoda, Y. Ueda, L.W. Anderson and J.E. Lawler, *Diam. Rel. Mater*. 1994, **3**, 422-425.

[15] P. Hartmann, R. Haubner and B. Lux, *Diam. Rel. Mater*. 1996, **5**, 850-856.

[16] Yu.A. Mankelevich, A.T. Rakhinov, N.V. Suetin and S.V. Kostyuk, *Diam. Rel. Mater*. 1996, **5**, 964-967.

[17] J.-K. Lee, K.Y. Eun, Y.-J. Baik, H.J. Cheon, J.W. Rhyu, T.J. Shin and J.-W. Park, *Diam. Rel. Mater*. 2002, **11**, 463-466.

[18] H.-J. Lee, H. Jeon and W.-S. Lee, *J. Appl. Phys*. 2011, **109**, 023303.

[19] K. Suzuki, A. Sawabe, H. Yasuda and T. Inuzuka, *Appl. Phys. Lett*. 1987, **50**, 728-729.

[20] K. Kurihara, K. Sasaki, M. Kawarada and N. Koshin, *Appl. Phys. Lett*. 1988, **52**, 437-438.

[21] V.I. Konov, A.A. Smolin, V.G. Ralchecko, S.M. Pimenov, E.D. Obraztsova, E.N. Loubnin, S.M. Metev and G. Sepold, *Diam. Rel. Mater*. 1995, **4**, 1073-1078.

[22] J. Luque, W. Juchmann, E.A. Brinkman and J.B. Jeffries, *J. Vac. Sci. Tech. A*, 1998, **16**, 397-408.

[23] F.X. Lu, W.Z. Tang, T.B. Huang, J.M. Liu, J.H. Song, W.X. Yu and Y.M. Tong, *Diam. Rel. Mater*. 2001, **10**, 1551-1558.

[24] J.B. Wills, J.A. Smith, W.E. Boxford, J.M.F. Elks, M.N.R. Ashfold and A.J. Orr-Ewing, *J. Appl. Phys*. 2002, **92**, 4213-4222.

[25] F.G. Celii and J.E. Butler, *Ann. Rev. Phys. Chem*. 1991, **42**, 643-684.

[26] D.G. Goodwin and J.E. Butler, in *Handbook of Industrial Diamonds and Diamond Films*, (eds. M.A. Prelas, G. Popovici and L.G. Bigelow), Marcel Dekker, New York, 1998, pp. 527-581.

[27] A. Gicquel, K. Hassouni, F. Silva and J. Achard, *Curr. Appl. Phys*. 2001, 1, 479-496.

[28] P.W. May, *Phil. Trans. R. Soc. London, Ser. A* 2000, **358**, 473-495.

[29] M.N.R. Ashfold, P.W. May, J.R. Petherbridge, K.N. Rosser, J.A. Smith, Yu.A. Mankelevich and N.V. Suetin, *Phys. Chem. Chem. Phys*. 2001, **3**, 3471-3485.

[30] T. Teraji, *Phys. Status Solidi* 2006, **203**, 3324-3357.

[31] J.E. Butler, Yu.A. Mankelevich, A. Cheesman, J. Ma and M.N.R. Ashfold, *J. Phys.: Condens. Matter*, 2009, **21**, 364201.

[32] D.S. Knight and W.B. White, *J. Mater. Res*. 1989, **4**, 385-393.

[33] A.C. Ferrari and J. Robertson, *Phil. Trans. Roy. Soc. A*, 2004, **362**, 2477-2512.

[34] D.W. Comerford, J.A. Smith, M.N.R. Ashfold and Yu.A. Mankelevich, *J. Chem. Phys*. 2009, **131**, 044326.

[35] F.G. Celii and J.E. Butler, *Appl. Phys. Lett*. 1989, **54**, 1031-1033.

[36] L. Schafer, C.P.Klages, U. Meier and K. Hohse-Höinghaus, *Appl. Phys. Lett*. 1991, **58**, 571-573.

[37] W.L. Hsu, *Appl. Phys. Lett*. 1991, **59**, 1427-1429.

[38] K.H. Chen, M.C. Chuang, C.M. Penney and W.F. Banholzer, *J. Appl. Phys*. 1992, **71**, 1485-1493.

[39] L.L. Connell, J.W. Fleming, H.N. Chu, D.J. Vestyck, E. Jensen and J.E. Butler, *J. Appl. Phys*. 1996, **78**, 3622-3634.

[40] S.A. Redman, C. Chung, K.N. Rosser and M.N.R. Ashfold, *Phys. Chem. Chem. Phys*. 1999, **1**, 1415-1424.

[41] E.H. Wahl, T.G. Owano, C.H. Kruger, P. Zalicki and R.N. Zare, *Diam. Rel. Mater*. 1997, **6**, 476-480.

[42] J.A. Smith, E. Cameron, M.N.R. Ashfold and Yu.A. Mankelevich, *Diam. Rel. Mater*. 2001, **10**, 358-363.

[43] D.G. Goodwin and G.G. Gavillet, *J. Appl. Phys*. 1990, **68**, 6393-6400.

[44] J. Ma, J.C. Richley, M.N.R. Ashfold and Yu.A. Mankelevich, *J. Appl. Phys*. 2008, **104**, 103305.

[45] J. Ma, M.N.R. Ashfold and Yu.A. Mankelevich, *J. Appl. Phys*. 2009, **105**, 043302.

[46] J. Ma, A. Cheesman, M.N.R. Ashfold, K.G. Hay, S. Wright, N. Langford, G. Duxbury and Yu.A. Mankelevich, *J. Appl. Phys*. 2009, **106**, 033305.

[47] G. Lombardi, K. Hassouni, F. Benedic, F. Mohasseb, J. Röpcke and A. Gicquel, *J. Appl. Phys*. 2004, **96**, 6739-6751.

[48] G. Lombardi, G.D. Stancu, F. Hempel, A. Gicquel and J. Röpcke, *Plasma Sources Sci. Technol*. 2004, **13**, 27-38.

[49] G. Lombardi, K. Hassouni, G.D. Stancu, L. Mechold, J. Röpcke and A. Gicquel, *Plasma Sources Sci. Technol*. 2005, **14**, 440-450.

[50] A. Cheesman, J.A. Smith, M.N.R. Ashfold, N. Langford, S. Wright and G. Duxbury, *J. Phys. Chem A* 2006, **110**, 2821-2828.

[51] C. Rond, S. Hamann, M. Wartel. G. Lombardi, A. Gicquel and J. Röpcke, *J. Appl. Phys*. 2014, **116**, 093301.

[52] M.A. Cappelli, T.G. Owano, A. Gicquel and X. Duten, *Plasma Chem. Plasma Proc*. 2000, **20**, 1-12.

[53] P. John, J.R. Rabeau and J.I.B. Wilson *Diam. Rel. Mater.* 2002, **11**, 608-11.

[54] J. Ma, J.C. Richley, D.R.W. Davies, M.N.R. Ashfold and Yu.A. Mankelevich, *J. Phys. Chem. A.* 2010, **114**, 10076-10089.

[55] J.C. Richley, O.J.L. Fox, M.N.R. Ashfold and Yu.A. Mankelevich, *J. Appl. Phys*. 2011, **109**, 063307.

[56] M.W. Kelly, J.C. Richley, C.M. Western, M.N.R. Ashfold and Yu.A. Mankelevich, *J. Phys. Chem. A* 2012, **116**, 9431-9446.

[57] B.S. Truscott, M.W. Kelly, K.J. Potter, M.N.R. Ashfold and Yu.A. Mankelevich, *J. Phys. Chem. A* 2016, **120**, 8537-8549.

[58] J.W. Coburn and M. Chen, *J. Appl. Phys.* 1980, **51**, 3134-3136.

[59] A. Gicquel, M. Chenevier and M. Lefebvre, in *Handbook of Industrial Diamonds and Diamond Films*, (eds. M.A. Prelas, G. Popovici and L.G. Bigelow), Marcel Dekker, New York, 1998, pp. 739-796.

[60] A. Gicquel, M. Chenavier, K. Hassouni, A. Tserepi and M. Dubus, *J. Appl. Phys.* 1998, **83**, 7504-7521.

[61] H. Yamada, *Jpn. J. Appl. Phys*. 2012, **51**, 090105

[62] S.V. Kostiuk, Yu.A. Mankelevich, A.T. Rakhimov and N.V. Suetin, *Proc. 5th. Int. Symp. on Diamond Materials*, (ed. J.L. Davidson, The Electrochem. Soc., Paris, France) 1997, 152-160.

[63] K. Hassouni, T.A.Grotjohn and A. Gicquel, *J. Appl. Phys.* 1999, **86**, 134-151.

[64] A.M. Gorbachev, V.A. Koldanov and A. Vikharev, *Diam. Rel. Mater*. 2001, **10**, 342-346.

[65] H. Yamada, A. Chayahara and Y. Mokano, *J. Appl. Phys.* 2007, **101**, 063302.

[66] Yu.A. Mankelevich and P.W. May, *Diam. Rel. Mater*. 2007, **17**, 1021-1028.

[67] Yu.A. Mankelevich, M.N.R. Ashfold and J. Ma, *J. Appl. Phys*. 2008, **104**, 113304.

[68] P.W. May and Yu.A. Mankelevich, *J. Phys. Chem. C* 2008, **112**, 12432-12441.

[69] J.C. Richley, O.J.L. Fox, M.N.R. Ashfold and Yu.A. Mankelevich, *J. Appl. Phys*. 2011, **109**, 063307.

[70] J. Ma, J.C. Richley, D.R.W. Davies, A. Cheesman, M.N.R. Ashfold and Yu.A. Mankelevich, *J. Phys. Chem. A.* 2010, **114**, 2447-2463.

[71] B.S. Truscott, M.W. Kelly, K.J. Potter, M. Johnson, M.N.R. Ashfold and Yu.A. Mankelevich, *J. Phys. Chem. A* 2015, **119**, 12962-12976.

[72] J.C. Richley, M.W. Kelly, M.N.R. Ashfold and Yu.A. Mankelevich, *J. Phys. Chem. A* 2012, **116**, 9447-9458.

[73] A.G. Engelhardt and A.V. Phelps, *Phys. Rev.* 1963, **131**, 2115-2128.

[74] K. Hassouni, A. Gicquel, M. Capitelli and J. Louriero, *Plasma Sources Sci. Technol*. 1999, **8**, 494-512.

[75] G. Lombardi, K. Hassouni, G. D. Stancu, L. Mechold, J. Ropcke and A. Gicquel, *J. Appl. Phys.* 2005, **98**, 053303.

[76] J.O. Hirschfelder, C.F. Curtiss and R.B. Bird, *Molecular Theory of Gases and Liquids* (John Wiley and Sons, Inc., New York, 1954), p. 1110.

[77] D.S. Dandy and M.E. Coltrin, *J. Mater. Res*. 1995, **10**, 1993-2010.

[78] C_2 radicals are normally monitored in their low lying $a^3\Pi_u$ excited state rather than the $X^1\Sigma_g^+$ ground state – both because it is operationally more convenient, and because the 6-fold higher multiplicity ensures that most C_2 radicals in a sample at T_{gas} ~3000 K will be in the former state. See C.J. Rennick, J.A. Smith, M.N.R. Ashfold and A.J. Orr-Ewing, *Chem. Phys. Lett*. 2004, **383**, 518-522.

[79] S.J. Harris, *Appl. Phys. Lett.* 1990, **23**, 2298-2300.

[80] M. Frenklach and H. Wang, *Phys. Rev. B* 1991, **43**, 1520-1545.

[81] B.J. Garrison, E.J. Dawnkaski, D. Srivistava and D.W. Brenner, *Science* 1992, **256**, 835-838.

[82] J.E. Butler and R.L. Woodin, *Phil. Trans. Roy. Soc. A* 1993, **342**, 209-224.

[83] S. Skokov, B. Weiner and M. Frenklach, *J. Phys. Chem*. 1994, **98**, 7073-7082.

[84] H. Tamura, H. Zhou, Y. Hirano, S. Takami, M. Kubo, R.V. Belosludov, A. Miyamoto, A. Imamura, M.N. Gamo and T. Ando, *Phys. Rev. B* 2000, **62**, 16995-17003.

[85] A. Cheesman, J.N. Harvey and M.N.R. Ashfold, *J. Phys. Chem. A* 2008, **112**, 11436-11448.

[86] J.C. Richley, J.N. Harvey and M.N.R. Ashfold, *J. Phys. Chem. C* 2012, **116**, 7810-7816.

[87] A. Gicquel, K, Hassouni, F. Silva and J. Achard, *Curr. Appl. Phys.* 2001, **1**, 479-496.

[88] A. Deneuville, *Semiconductors and Semimetals*, 2003, **76**, 183-238.

[89] J.E. Butler, A. Vikharev, A. Gorbachev, M. Lobaev, A. Muchnikov, D. Radischev, V. Isaev, V. Chernov, S. Bogdanov, M. Drozdov, E. Demidov, E. Surovegina, V. Shashkin, A. Davidov, H.-Y. Tan, L. Meshi, A.C. Pakpour-Tabrizi, M.-L. Hicks and R.B. Jackman, *Phys. Status Solidi RRL*. 2017, **11**, 1600329.

[90] M. Osiac, B.P. Lavrov and J. Röpcke, *J. Quant. Spectrosc. Radiat. Transfer* 2002, **74**, 471-491.

[91] B.P. Lavrov, M. Osiac, A.V. Pipa and J. Röpcke, *Plasma Sources Sci. Technol.* 2003, **12**, 576-589.

[92] S. Hamann, C. Rond, A.V. Pipa, M. Wartel, G. Lombardi, A. Gicquel and J. Röpcke, *Plasma Sources Sci. Technol.* 2014, **23**, 045015.

[93] C. Rond, R.Salem, S. Hamann, G. Lombardi, J. Röpcke and A. Gicquel, *Plasma Sources Sci. Technol.* 2016, **25**, 025016.

[94] M. Rayar, P. Veis, C. Foissac, P. Supiot and A. Gicquel, *J. Phys. D: Appl. Phys.*, 2006, **39**, 2151-2159.

[95] M. Rayar, P. Supiot, P. Veis and A. Gicquel, *J. Appl. Phys.* 2008, **104**, 033304.

[96] A. Cheesman, J.N. Harvey and M.N.R. Ashfold, *Phys. Chem. Chem. Phys.* 2005, **7**, 1121-1126.

[97] J.C. Richley, J.N. Harvey and M.N.R. Ashfold, *J. Phys. Chem. C*, 2012, **116**, 18300-18307.

[98] B.B. Li, M.C. Tosin, A.C. Peterlevitz and V. Baranauskas, *Appl. Phys. Lett*. 1998, **73**, 812-814.

[99] S. Jin and T.D. Moustakas, *Appl. Phys. Lett.* 1994, **65,** 403-405.

[100] W. Müller-Sebert, E. Wörner, F. Fuchs, C. Wild and P. Koidl, *Appl. Phys. Lett.* 1996, **8**, 759-760.

[101] C.-S. Yan, Y.K. Vohra, H.-K. Mao and R.J. Hemley, *Proc. Nat. Acad. Sci*. 2002, **99**, 12523-12525.

[102] A. Chayahara, Y. Mokuno, Y. Horino, Y. Takasu, H. Kato, H. Yoshikawa and N. Fujimori, *Diam. Rel. Mater*. 2004, **13**, 1954-1958.

[103] Y. Liu and D. Raabe, *Appl. Phys. Lett*. 2009, **94**, 021119.

[104] J. Achard, F. Silva, O. Brinza, A. Tallaire and A. Gicquel, *Diam. Rel. Mater*. 2007, **16**, 685-689.

[105] S. Dunst, H. Sternschulte and M. Schreck, *Appl. Phys. Lett*. 2009, **94**, 224101.

[106] Y.J. Gu, J. Lu, T. Grotjohn, T. Schuelke and J. Asmussen, *Diam. Rel. Mater*. 2012, **24**, 210-214.

[107] J. Lu, Y. Gu, T.A. Grotjohn, T. Schuelke and J. Asmussen, *Diam. Rel. Mater*. 2013, **37**, 17-28.

[108] S. Bogdanov, A. Vikharev, A. Gorbachev, A. Muchnikov, D. Radishev, N. Ovechkin and V. Parshin, *Chem. Vapor Depos.* 2014, **20**, 32-38.

[109] G.Z. Cao, J.J. Schermer, W.J.P. van Enckevort and W.A.L.M. Elst and L.J. Giling, *J. Appl. Phys*. 1996, **79**, 1357-1364.

[110] Y. Avigal, O. Glozman, I. Etsion, G. Halperin and A. Hoffmann, *Diam. Rel. Mater*. 1997, **6**, 381-385.

[111] C.J. Tang, A.J.S. Fernandes, F. Costa and J.L. Pinto, *Vacuum*, 2011, **85**, 1130-1134.

[112] B.S. Truscott, M.W. Kelly, K.J. Potter, M. Johnson, M.N.R. Ashfold and Yu.A. Mankelevich, *J. Phys. Chem. A* 2015, **119**, 12962-12976.

[113] M.W. Kelly, S.C. Halliwell, W.J. Rodgers, J.D. Pattle, J.N. Harvey and M.N.R. Ashfold, *J. Phys. Chem. A* 2017, **121**, 2046-2055.

[114] Z. Yiming, F. Larsson and K. Larsson, *Theor. Chem. Acc*. 2014, **133**, 1432.

[115] T. Kawato and K. Kondo, *Jap. J. Appl. Phys*. 1987, **26**, 1429-1432.

[116] S.J. Harris and A.M. Weiner, *Appl. Phys. Lett*. 1989, **55**, 2179-2181.

[117] Y. Muranaka, H. Yamashita, K. Sato and H. Miyadera, *J. Appl. Phys*. 1990, **67**, 6247-6254.

[118] G. Balestrino, M. Marinelli, E. Milani, A. Paoletti, I. Pinter and A. Tebano, *Appl. Phys. Lett*. 1993, **62**, 879-881.

[119] C.F. Chen, S. Chen, H. Ko and S.E. Hsu, *Diam. Rel. Mater*. 1994, **3**, 443-447.

[120] J. Stiegler, T. Lang, M. Nygard-Ferguson, Y. von Kaenel and E. Blank, *Diam. Rel. Mater*. 1996, **5**, 226-230.

[121] T.P. Mollart and K.L. Lewis, *Diam. Rel. Mater*. 1999, **8**, 236-241.

[122] J.R. Petherbridge, P.W. May, S.R.J. Pearce, K.N. Rosser and M.N.R. Ashfold, *J. Appl. Phys*. 2001, **89**, 1484-1492.

[123] P.K. Bachmann, D. Leers and H. Lydtin, *Diam. Rel. Mater*. 1991, **1**, 1-12.

[124] E.J.D. Mahoney, B.S. Truscott, M.N.R. Ashfold and Yu.A. Mankelevich, *J. Phys. Chem. A* 2017, **121**, 2760-2772.

[125] A. Netto and M. Frenklach, *Diam. Rel. Mater*. 2005, **14**, 1630-1646.

[126] M. Eckert, E. Neyts and A. Bogaerts, *Cryst. Growth and Design*, 2010, **10**, 3005-3021.

[127] W.J. Rodgers, P.W. May, N.L. Allan and J.N. Harvey, *J. Chem. Phys*. 2015, **142**, 214707.

[128] D.G. Goodwin, *J. Appl. Phys*. 1993, **74**, 6888-6894.

[129] N. Derkaoui, C. Rond, K. Hassouni and A. Gicquel, *J. Appl. Phys*. 2014, **115**, 233301.

[130] A. Gicquel, N. Derkaoui, C. Rond, F. Benedic, G. Cicala, D. Monegar and K. Hassouni, *Chem. Phys*. 2012, **398**, 239-247.

[131] K.W. Hemawan, T.A. Grotjohn, D.K. Reinhard and J. Asmussen, *Diam. Rel. Mater*. 2010, **19**, 1446-1452.

[132] S. Nad, Y.J. Gu and J. Asmussen, *Rev. Sci. Instrum*. 2015, **86**, 074701.